J Mater Sci (2009) 44:2931–2937
DOI 10.1007/s10853-009-3388-9

Deposition of thin cobalt films onto silicon by galvanostatic and potentiostatic techniques

Taíse Matte Manhabosco · Iduvirges L. Müller

Received: 7 January 2008 / Accepted: 5 March 2009 / Published online: 31 March 2009

Abstract In this study, thin cobalt films were electrodeposited directly onto *n*-Si (100) using two different electrodeposition techniques: galvanostatic and potentiostatic. The morphological difference between galvanostatic and potentiostatic deposits was observed by atomic force microscopy (AFM) and X-ray diffraction (XRD). Analysis of the deposits by an alternating gradient field magnetometer (AGFM) showed the influence of the electrodeposition process on the magnetic properties of the film.

Introduction

In the last 30 years the attention of research has moved from micro to nanosized materials. On a nanosized scale the properties suffer the quantum phenomenon influence that enables obtaining properties different from those gained with the same bulk material [1–3].

An important class of nanosized materials that has been investigated intensively is that of thin magnetic films and their multilayers. Their unusual properties, such as perpendicular magnetic anisotropy and giant magnetoresistance promoted a major technological advance. Perpendicular magnetic anisotropy enables the high recording density besides favoring the reading of the recorded data. Giant magnetoresistance has a potential application in magnetic data recording and magnetic field sensing.

T. M. Manhabosco (✉) · I. L. Müller
Laboratory of Corrosion Research, Metallurgy Department, Universidade Federal do Rio Grande do Sul, Av. Bento Gonçalves 9500/Setor 4/Prédio 75/232, Porto Alegre 91501-970, Rio Grande do Sul, Brazil
e-mail: tmanhabosco@yahoo.com.br

Thin films are commonly obtained through physical methods like physical vapor deposition (PVD), chemical vapor deposition (CVD), sputtering, and others [4–7]. Despite the adequate film quality, these techniques have a relatively high cost and requirements like a vacuum system. An older technique, electrodeposition, which historically emphasized decorative applications and corrosion protection began to be used effectively for thin film production [8–17]. A promising future can be expected for this technique thanks to physical methods, such as its operation under normal conditions of pressure and temperature, at a relatively low cost and with thickness control by charge transfer in the process [2, 3, 18]. Furthermore, a number of parameters like pH, bath composition, stirring, additives, external magnetic field, continuous or pulsed current electrodeposition, can be adjusted in order to improve film quality and properties [9, 19–24]. With respect to the electrochemical deposition advantages, it is possible, as shown by Spoddig et al. [25], to perform in situ deposition during the ferromagnetic resonance (FMR) measurements with further information about the anisotropy and magnetization distribution.

Usually, the substrate used as a cathode is a conducting substrate. An insulating or semiconductor substrate requires a conducting seed layer to allow electrodeposition. However, if an *n*-doped semiconductor is used which conducts through the conduction band, the preparation step of the seed layer can be suppressed because the substrate may conduct sufficiently well to allow the electrodeposition directly onto it. Electrodeposition onto semiconductors also allows a selective growth of metallic films directly on pre-structured semiconductor substrates either by scratching the native oxide layer [26, 27], or using a focused ion beam [28]. Also focused light beam illumination of a semiconductor substrate has been reported to induce

selective metal deposition at the illuminated regions of the substrates [29–31]. The electrolytic deposition directly on a semiconductor substrate, by forming a layer or dots, can promote integration between the semiconductor microelectronic technology and the electrodeposition technique.

Many studies used the potentiostatic technique [10, 12, 16, 23, 24, 32–38] in order to obtain electrodeposition of films onto silicon, while the galvanostatic technique [11, 29, 39] has been less frequently reported in the literature. In a previous work [40], we have predicted the nucleation behavior and shown the influence of *n*-type semiconductor resistivity on the potentiostatic and galvanostatic deposition, as well as on the cobalt films morphology. For the potentiostatic deposits the silicon resistivity plays a role, while for the galvanostatic deposits it was not observed significant influence on cobalt nuclei morphology, possibly because in the galvanostatic method the deposition is constrained to occur at an imposed rate. By adding saccharin to the electrodeposition solution the morphology, crystallographic structure, and magnetic behavior of potentiostatically deposited cobalt films showed a finer morphology, a single hexagonal close-packed phase and an in-plane magnetization [20].

In the present work, we compare potentiostatic and galvanostatic cobalt deposition in the early stages of deposition onto silicon. Cobalt was chosen because this metal and its alloys are ideal for digital recording since they can present uniaxial symmetry, even if this attribute strongly depends on preparation conditions which define the deposits crystallographic structure and consequent magnetic properties [41, 42].

Experimental

Monocrystalline *n*-silicon (100) wafers with resistivity $<0.005\ \Omega$cm were used as substrate. The 8×8 mm silicon samples polished on one side were obtained by cleaving from silicon wafers and passed through the RCA cleaning technique [43]. Prior to each experiment the samples were successively cleaned in acetone, methanol, and bi-distilled water. The ohmic contact of each sample with a 316 stainless steel holder was made through a metallic indium back contact. A hydrofluoric acid (HF) resistant polypropylene adhesive tape was used to determine an exposed area of 0.246 cm^2. The native surface oxide was removed before deposition by immersing the sample for 30 s in a 10% HF solution, followed by rinsing in bi-distilled water. After oxide removal, the surface was hydrophobic and H-terminated [44, 45].

The electrodeposition was performed in an aqueous solution containing 10 mM $CoSO_4 \cdot 7H_2O$, 10 mM K_2SO_4, 1 mM H_2SO_4, 0.1 mM KCl. The solution was prepared from bi-distilled water and analytical grade reagents and its pH value was 2.8. The temperature of the bath was 298($\pm$1) K. A platinum wire was used as counter electrode and a saturated calomel electrode (SCE) as reference electrode. All the experiments were performed in a dark Faraday cage in order to avoid the light and possible electromagnetic interferences.

Cyclic voltammetry was performed to characterize the system and establish the appropriate potentials or currents for deposition. The deposits were obtained from galvanostatic and potentiostatic techniques. For potentiostatic deposition a Gill AC potentiostat (ACM Instruments) was used and galvanostatic deposits were obtained using a EG&G PAR 273A potentiostat/galvanostat. The morphology of deposits was verified by an atomic force microscope (AFM) from SHIMADZU (model SPM-9500J3). X-ray diffraction (XRD) measurements were performed in order to determine the crystallographic structure. Magnetic hysteresis loops of the deposits were obtained using an alternating gradient field magnetometer (AGFM).

Results and discussion

A typical cyclic voltammogram of the system studied, performed by sweeping the potential first in cathodic then in anodic direction is shown in Fig. 1. A cathodic peak related to cobalt reduction can be seen, indicating that the deposition of cobalt becomes diffusion limited after nucleation has occurred. At more negative potentials, hydrogen evolution becomes considerable and the current increases again. Hydrogen evolution occurring concomitantly with cobalt reduction is reported by other authors [36] and was confirmed by cyclic voltammogram

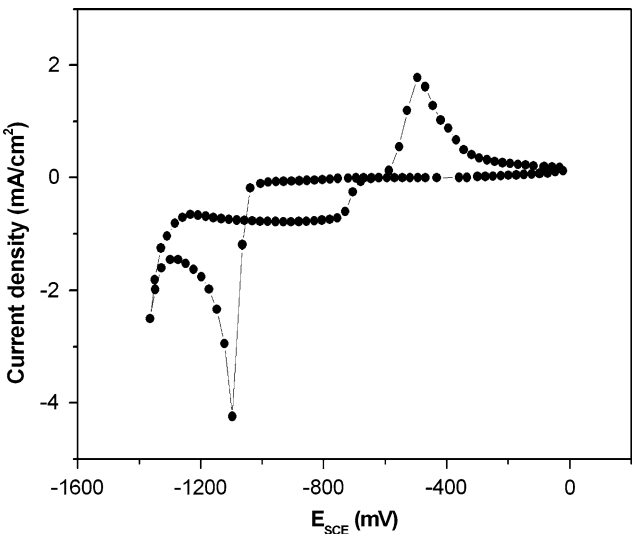

Fig. 1 Cyclic voltammetry in cobalt solution. Scan rate: 1200 mV/min

performed in a cobalt ion-free electrolyte that shows a high hydrogen evolution at potentials more negative than −1200 mV. Furthermore, it can be seen (Fig. 1) that the anodic charge is lower than the cathodic charge, which may be associated to a Schottky-barrier formation. The lower anodic charge and visual inspection of the surface after the cyclic voltammetry experiment allow the inference that some cobalt remains on the silicon surface.

Figure 2 shows chronogalvanometric transients for cobalt electrodeposition at −1000 mV, −1050 mV, −1100 mV, and −1150 mV. The curves for −1000 mV and −1050 mV show in the first moments a current peak that can be related to nucleation and growth mechanisms. For lower potentials the nucleation and growth became very fast and could not be recorded due to limitations of the equipment. The deposition rate increases with overpotentials and for longer times the current for all potential approaches to the same value, indicating that the growth is diffusion controlled.

Figure 3 shows an AFM image of the cobalt morphology obtained by potentiostatic deposition at −1150 mV during 39 s. Cobalt deposits as three-dimensional nuclei that are homogeneously distributed over the silicon surface. Nuclei are similar in size, possibly because after the initial nucleation, cobalt atoms prefer attaching to these nuclei instead of forming new ones. An idea of quantity can be obtained from the fact that nuclei show a diameter of about 230 nm and are 80 nm high. Some scarce smaller nuclei can be seen in the right corner that should have been formed latterly as preferential attachment of cobalt atoms to an existent nucleus do not exclude the possibility to form rare new ones. When the overpotential of deposition was decreased, it was observed an increase in the nuclei size and a decrease in the nuclei quantity.

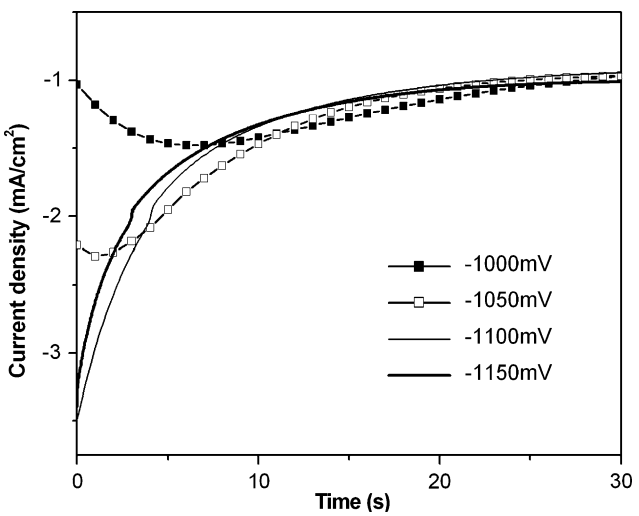

Fig. 2 Chronogalvanometric transients for cobalt electrodeposition at −1000 mV, −1050 mV, −1100 mV, −1150 mV

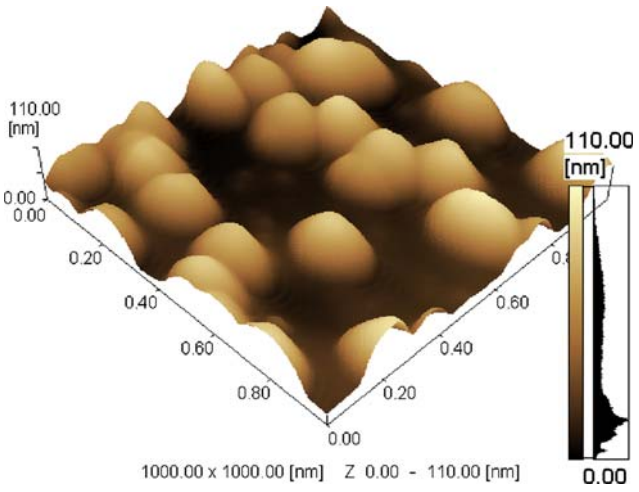

Fig. 3 AFM image of potentiostatic cobalt deposit obtained at −1150 mV for 39 s onto silicon

To achieve galvanostatic depositions, five different current densities were used and the acquired chronopotentiometic curves are shown in Fig. 4. At higher cathodic current densities, 4 mA/cm^2 and 8 mA/cm^2, the system imposes a high overpotential in which the hydrogen evolution is very expressive, as observed in the cyclic voltammogram. The curves, except for the applied current density of 1 mA/cm^2 present a "transition time" that indicates the beginning of the deposition controlled by diffusion. As expected, the higher the current density, the lower the "transition time".

In Fig. 5 are shown the galvanostatic deposits obtained at a cathodic current density of 1.5 mA/cm^2 after 30 s. This charge transferred during 30 s in galvanostatic deposition is equivalent to the charge transferred in the potentiostatic one at −1150 mV during 39 s; however, the thickness

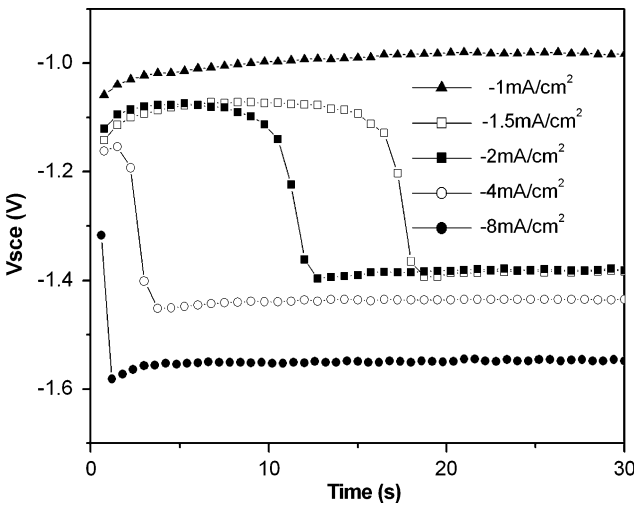

Fig. 4 Chronopotentiometric transients for cobalt electrodeposition at cathodic current densities of 1 mA/cm^2, 1.5 mA/cm^2, 2 mA/cm^2, 4 mA/cm^2 and 8 mA/cm^2

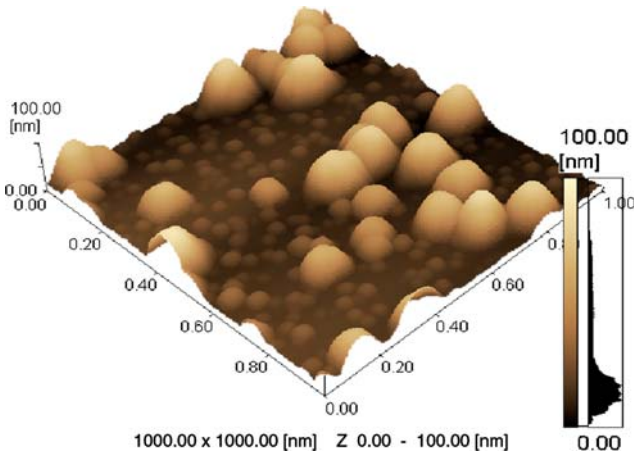

Fig. 5 AFM image of galvanostatic cobalt deposit obtained at a cathodic current of 1.5 mA/cm^2 for 30 s

probably is not the same as the deposition processes are different. It can be clearly seen that the deposits present basically two different-sized nuclei groups; the smaller ones being about 30 nm in diameter while the larger are about 130 nm. However, when the depositions were carried out during only 15 s, time inferior to the "transition time", the deposits present just one size nuclei group. In order to investigate this occurrence, deposition was carried out during 30 s with a current density with which the "transition time" is not observed. Figure 6 presents a deposit obtained at 1 mA/cm^2 where just one size of nuclei being about 160–180 nm in diameter is to be found. Probably, by these observations, the smaller nuclei are formed after the "transition time" when the driving force for nucleation is higher.

The determination of the potentiostatic deposits structure by XRD revealed that both hexagonal close-packed (hcp) and faced-centered cubic (fcc) phases are formed under potentiostatic deposition conditions (Fig. 7). Due to

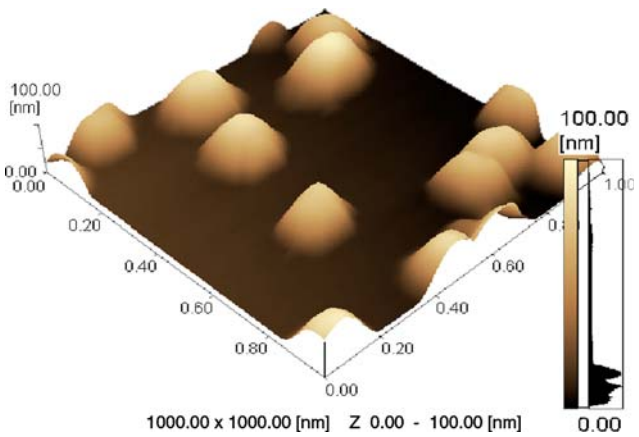

Fig. 6 AFM image for galvanostatic cobalt deposit obtained at a cathodic current of 1 mA/cm^2 for 30 s

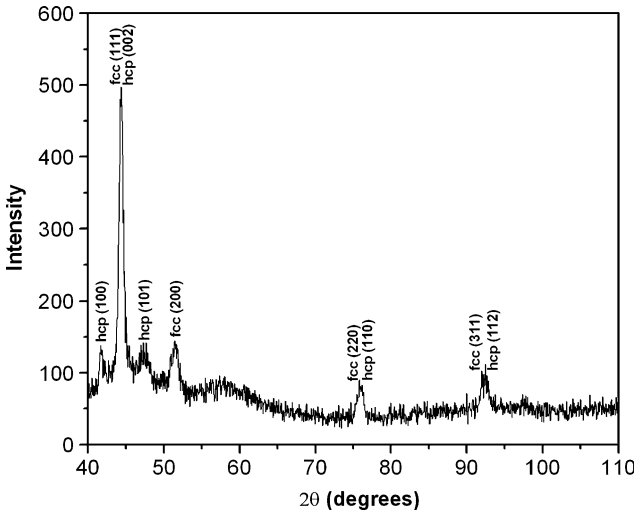

Fig. 7 X-ray spectrum of potentiostatic cobalt deposit obtained at −1150 mV

the small thickness of the deposits, which is about 70 nm, a widening of the diffraction peaks is observed because there is no long-range periodicity. Furthermore, some peaks of hcp and fcc phases are located at angles that are very close together; therefore they appeared as only one peak in the spectrum, which presented as wider and stronger due to this superposition. In the XRD spectrum the peaks (100), (002), (101), (110), and (112) from the hcp phase and the (100), (111), (200), (220), (311) peaks from the fcc phase are identified. Some peaks are not present and others differ in intensity from the peaks of a random distribution as can be seen by the preferential fcc [111] and hcp [002] textures, as compared to the other textures. Vicenzo and Cavallotti [21] suggest a progressive formation of hcp cobalt as pH decreases and the presence of hcp (002) and fcc (111) reflections were found in buffered solutions just at pH < 3.2. The preferential orientation in the electrodeposition process is a very well-known occurrence and is to be related to the operative conditions like solution composition and concentration, pH, temperature, and material substrate [8, 9, 46–48].

In galvanostatic deposits obtained at a cathodic current of 1.5 mA/cm^2, with a mean calculated thickness about 200 nm, only one peak from the fcc phase was found with (111) orientation (Fig. 8). According to the XRD spectrum results, the galvanostatic deposits are characterized by the absence of periodic scatter centers, consisting mainly of an amorphous structure.

Magnetic hysteresis loops of potentiostatically deposited films, which present the two crystallographic modifications of cobalt: hcp and fcc, were measured applying magnetic field parallel and perpendicular to the plane of the film at room temperature. These two phases are very different with respect to their ferromagnetic properties, hcp cobalt having

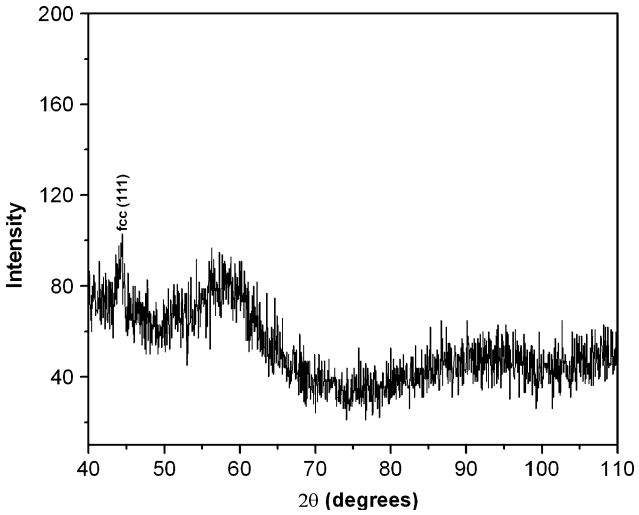

Fig. 8 X-ray spectrum of galvanostatic deposit of cobalt obtained at a cathodic current of 1.5 mA/cm^2

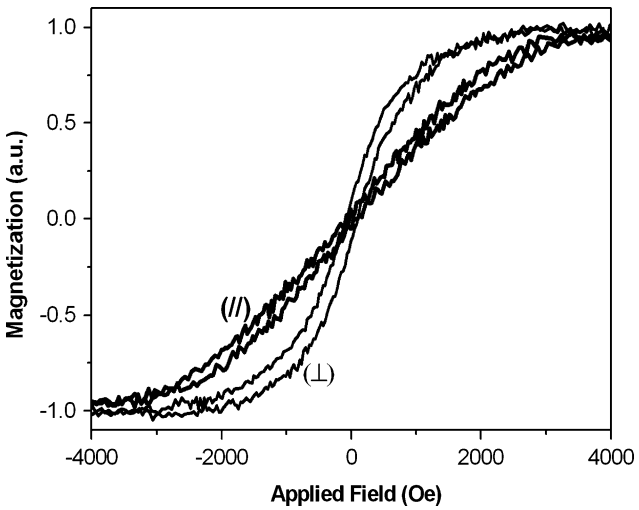

Fig. 9 Magnetization curve for cobalt film deposited potentiostatically. The magnetic field applied was parallel (||) or perpendicular (⊥) to the deposit

only one axis of easy magnetization [001], whereas fcc cobalt has four easy axis [111]. Figure 9 presents the characteristic M-H curves for a potentiostatic deposit, with a mean calculated thickness about 70 nm. The magnetic curve in the parallel configuration shows an absence of hysteresis and has a linear response at small fields. The almost complete absence of remanence (Mr = 0.025 a.u.) is well-related to a superparamagnetic behavior. However, the nuclei size of the potentiostatic cobalt deposits, about 230 nm, is too large to justify this kind of behavior [49]. One possibility of explanation, is that the plane magnetic moment components of different domains cancel one each other in absence of an external field ($H = 0$). Nevertheless, when the magnetic field was perpendicularly applied to the plane of the film a ferromagnetic response was obtained and the M-H loop shows a Mr about 0.1. The magnetic behavior shows that the cobalt films potentiostatically deposited are well-related to an anisotropic material. Bubendorf et al. [23] have found in ultrathin cobalt films electrodeposited on Au (111) that the magnetic behavior is related to the film thickness and potential deposition. Films obtained at −180 mV have a strongest magnetization component along the parallel direction of the film, while films obtained at −680 mV have a strongest magnetization component along the perpendicular direction similarly as presented by our films deposited at −1150 mV. For very thin films (<7 atomic layers) deposited at −680 mV, the authors verified a clear magnetization perpendicular to the films plane which is expressed by the rectangular shape of the hysteresis loop. As the film thickness is increased the opening of the loop is stretched out.

In a recent report [20], we have shown that the presence of saccharin additive to the electrodeposition solution, on the contrary of the dual-phase structure, produces cobalt films with a single hcp phase structure. The magnetic response to an applied magnetic field parallel to the film plane was also changed from the behavior presented in the Fig. 9 to a rectangular shape of the hysteresis loop as the

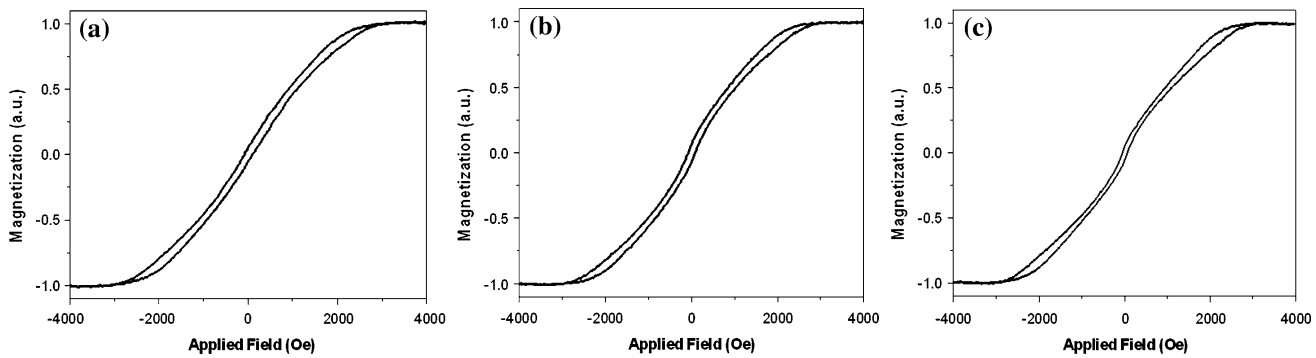

Fig. 10 Magnetization curves for cobalt films deposited galvanostatically. The magnetic field applied was parallel to the deposit. Times of deposition: (**a**) 15 s; (**b**) 30 s; (**c**) 40 s

concentration of saccharin was increased indicating an in-plane magnetization.

Figure 10 shows the magnetic behavior for the different galvanostatic deposits; the measurements were performed applying magnetic field parallel to the plane of the film at room temperature. Figure 10a shows the magnetic behavior for a deposit obtained during 15 s of deposition, time just before the "transition time" and which corresponds to an "equivalent" thickness of just 32 nm. Figure 10b and c shows the magnetic behavior for galvanostatic deposits obtained during 30 and 40 s, corresponding to about 64 nm and 85 nm calculated film thickness, respectively. The magnetic behavior of the galvanostatic deposits is different from that presented by the potentiostatic ones. For galvanostatic deposits Fig. 10b and c, the hysteresis loop presents a central region with a different inclination from the rest of the loop while the hysteresis loop presented in Fig. 10a, does not present this different inclination. The central differentiated inclination region becomes more important, as the film thickness increases, i.e., as the small nuclei grow at higher overpotentials. Thus, comparing the magnetic behavior with the AFM images and current transients, it can be proposed that the small nuclei forming after the "transition time" are responsible for the central inclination region in the magnetic curves. The occurrence of two different regions in the hysteresis loop may be ascribed to the existence of two different nuclei sizes.

As observed by the magnetic measurements, magnetic behavior is strongly dependent on the electrodeposition technique, what can be associated to the crystallographic and morphological structure of the deposits.

Conclusions

The present work shows the great influence exerted by the electrodeposition technique (galvanostatic or potentiostatic) on the morphology, microstructure and magnetic properties of cobalt films on silicon.

Cobalt deposits as tridimensional nuclei and concomitantly with the deposition hydrogen evolution occur. Comparing the film morphology, the potentiostatic deposits present more uniform-sized nuclei, while the galvanostatic deposits show two main groups of nuclei sizes.

The microstructure of potentiostatic deposits presents preferential orientation and both hexagonal close-packed (hcp) and faced-centered cubic (fcc) phases. The galvanostatic deposits are mainly amorphous.

Thus, like the morphology and the microstructure, the magnetic behavior is also different for galvanostatic and potentiostatic deposits. While the potentiostatic deposits present linear behavior in a small field and almost an absence of remanence when the applied magnetic field was parallel to the plane of the film, the galvanostatic deposits show a magnetic hysteresis loop with two different inclinations on the loop, associated with two different sizes of metallic nuclei.

References

1. McHenry ME, Laughlin DE (2000) Acta Mater 48:223
2. Osaka T, Homma T (1995) Electrochem Soc Interface 4(2):42
3. Switzer JA, Sheppard KG (1995) Electrochem Soc Interface 4(2):26
4. Baibich MN, Broto JM, Fert A, Nguyen Van Dau F, Petroff F (1988) Phys Rev Lett 61(21):2472
5. Ingvarsson S, Xiao G, Parkin SSP, Gallagher WJ (2002) J Magn Magn Mater 251:202
6. Oepen HP, Lutzke W, Kirschner J (2002) J Magn Magn Mater 251:169
7. Berkowitz AE, Mitchell JR, Carey MJ, Young AP, Zhang S, Spada FE, Parker FT, Hutten A, Thomas G (1992) Phys Rev Lett 68(25):3745
8. Gomez E, Vallés E (2002) J Appl Electrochem 32:693
9. Lallemand F, Ricq L, Wery M, Berçot P, Pagetti J (2004) Surf Coat Technol 179:314
10. Munford ML, Sartorelli ML, Seligman L, Pasa AA (2002) J Electrochem Soc 149(5):C274
11. Gao LJ, Ma P, Novogradecz KM, Norton PR (1997) J Appl Phys 81(11):7595
12. Reitzle A, Renner FU, Lee TL, Zegenhagen J, Kolb DM (2005) Surf Sci 576:19
13. Jyoko Y, Kashiwabara S, Hayashi Y (1997) J Electrochem Soc 144(7):L193
14. Jyoko Y, Schwarzacher W (2001) Electrochim Acta 47:371
15. Zangari G, Bozzini B, Cavallotti PL, Fontana G, Maisto PG, Terrenzio E (1994) J Magn Magn Mater 133:511
16. Shima M, Salamanca-Riba L, McMichael RD, Moffat TP (2002) J Electrochem Soc 149(9):C439
17. Georgescu V, Mazur V, Pushcashu B (2000) Mater Sci Eng B 68:131
18. Switzer JA (1998) Electrochem Soc Interface 7(1):23
19. Cho JU, Min JH, Ko SP, Soh JY, Kim YK, Wu J-H, Choi SH (2006) J Appl Phys 99:08C909
20. Manhabosco TM, Muller IL (2008) Surf Coat Tech 202:3585
21. Vicenzo A, Cavallotti PL (2004) Electrochim Acta 49:4079
22. Osaka T, Sawaguchi T, Mizutani F, Yokoshima T, Takai M, Okinaka Y (1999) J Electrochem Soc 146(9):3295
23. Bubendorff JL, Beaurepaire E, Meny C, Panissod P, Bucher JP (1997) Phys Rev B 56(12):R7120
24. Bubendorff JL, Beaurepaire E, Meny C, Bucher JP (1998) J Appl Phys 83(11):7043
25. Spoddig D, Meckenstock R, Bucher JP, Pelzl J (2005) J Magn Magn Mater 285:286
26. Schmuki P, Erickson LE (2000) Phys Rev Lett 85:2985
27. Santinacci L, Djenizian T, Schmuki P (2001) Appl Phys Lett 79:1882
28. Rastei MV, Meckenstock R, Devaux E, Ebbesen Th, Bucher JP (2005) J Magn Magn Mater 286:10
29. Scheck C, Liu Y-K, Evans P, Schad R, Bowers A, Zangari G, Williams JR, Issacs-Smith TF (2004) Phys Rev B 69:035334
30. Rose TL, Longendorfer DH, Rauh RD (1983) Appl Phys Lett 42:193
31. Diesinger H, Bsiesy A, Herino R (2001) J Appl Phys 90(9):4862
32. Zambelli T, Munford ML, Pillier F, Bernard M-C, Allongue P (2001) J Electrochem Soc 148(9):C614

33. Oskam G, Searson PC (2000) J Electrochem Soc 147(6):2199
34. Moina CA, de Oliveira-Versic L, Vazdar M (2004) Mater Lett 58:3518
35. Rashkova B, Guel B, Pötzschke RT, Staikov G, Lorenz WJ (1998) Electrochim Acta 43:3021
36. Pasa AA, Schwarzacher W (1999) Phys Status Solidi 173:73
37. Krumm R, Guel B, Schmitz C, Staikov G (2000) Electrochim Acta 45:3255
38. Stiger RM, Gorer S, Craft B, Penner RM (1999) Langmuir 15:790
39. Pattanaik GR, Pandya DK, Kashyap SC (2002) J Electrochem Soc 149(7):C363
40 Manhabosco T, Englert G, Muller IL (2006) Surf Coat Tech 200:5203
41. Yamada A, Houga T, Ueda Y (2002) J Magn Magn Mater 239:272
42. Sasaki H, Kainuma S, Takayanagi K, Hisatake K, Kim CO (2004) J Magn Magn Mater 281:53
43. Kern XW, Puotinen DA (1970) RCA Rev 31(2):187
44. Trucks GW, Raghavachari K, Higashi GS, Chabal YJ (1990) Phys Rev Lett 65(4):504
45. Morita Y, Tokumoto H (1995) Appl Phys Lett 67(18):2654
46. Armyanov S, Vitkova SD (1978) Surf Technol 7:319
47. Scoyer J, Winand R (1977) Surf Technol 5:169
48. Cardona L, Cavallotti P (1966) Electrochim Metall 1:364
49. Morup S, Tronc E (1994) Phys Rev Lett 72(20):3278